Hyperlabyrinth chaos: From chaotic walks to spatiotemporal chaos

Konstantinos E. Chlouverakis
Department of Informatics and Telecommunications, University of Athens, Athens 15784, Greece

J. C. Sprott
Departments of Physics, University of Wisconsin, Madison, Wisconsin 53706

(Received 12 July 2006; accepted 3 September 2007; published online 21 May 2007)

In this paper we examine a very simple and elegant example of high-dimensional chaos in a coupled array of flows in ring architecture that is cyclically symmetric and can also be viewed as an N-dimensional spatially infinite labyrinth (a "hyperlabyrinth"). The scaling laws of the largest Lyapunov exponent, the Kaplan–Yorke dimension, and the metric entropy are investigated in the high-dimensional limit ($3<N\leq 101$) together with its routes to chaos. It is shown that by tuning the single bifurcation parameter b that governs the dissipation and the number of coupled systems N, the attractor dimension can span the entire range of 0 to N including Hamiltonian (conservative) hyperchaos in the limit of $b=0$ and, furthermore, spatiotemporal chaotic behavior. Finally, stability analysis reveals interesting and important changes in the dynamics, whether N is even or odd.
 [DOI: 10.1063/1.2721237]

The study of chaotic dynamics has shifted during the last decade toward high-dimensional systems. Systems with a single bifurcation (control) parameter are especially preferred to serve as prototypical examples of high-dimensional chaos. Such simple systems could be delay differential equations (DDEs, such as the Mackey–Glass equation[1]) or partial differential equations (such as the Kuramoto–Sivashinsky equation[2]). Here, we focus on a system that can be viewed as a coupled system of N identical ordinary differential equations (ODEs) with a single control parameter whose basic characteristic is its ability to produce chaos, hyperchaos, and conservative (Hamiltonian) chaos by appropriate tuning, together with the number N of coupled systems. Furthermore, this system can be viewed as a one-dimensional ring resulting in spatiotemporal chaos, as a single trajectory on an N-dimensional torus, or as a single trajectory in an N-dimensional spatially infinite labyrinth (a "hyperlabyrinth").

I. INTRODUCTION

High-dimensional systems have received increasing attention in recent years since low-dimensional dynamics are now extensively studied.[3,4] Examples of such complex systems include time-delayed differential equations[1,5] and maps,[6] coupled three-dimensional flows such as Lorenz systems,[7] and many others. In this work, we deal with a system of N coupled ordinary differential equations (CODEs) in a ring architecture that was originally proposed by Thomas *et al.*[8] and that exhibits chaos even for the simplest case with $N=3$ (also further studied in Ref. 9) according to the Poincaré–Bendixson theorem[10] for which the conservative limit has been called "labyrinth chaos." Herein we study an obvious extension of this system, also suggested by Thomas *et al.*,[11] to higher dimensions ($3<N\leq 101$) (and therefore called "hyperlabyrinth chaos") given by

$$\frac{dx_i}{dt} = -bx_i + \sin x_{i+1} \tag{1}$$

with $i=1,2,\ldots,N$ and periodic boundary conditions $x_{N+1} \equiv x_1$. The system is cyclically symmetric in the variables x_i. The dissipation is governed by the parameter b, and the trace of the Jacobian matrix (the rate of state-space contraction) is always negative and equal to $-bN$; hence, $b>0$ for bounded solutions. A physical phenomenon that can be described by such a high-dimensional system could be a particle moving in an N-dimensional lattice (or "hyperlabyrinth") under the influence of some external source of energy. Furthermore, Eq. (1) is similar to the Ikeda delay differential equation[5] $dx(t)/dt=-bx(t)+\sin[x(t-\tau)]$, which is known to result in high-dimensional chaos and which is used for modeling lasers with wavelength hyperchaos.[12] The second bifurcation parameter τ (delay time) in the Ikeda DDE above coincides—in a manner of dynamical topology—with the number N of the coupled systems of Eq. (1) since the interval $[-\tau,0]$ in the DDE is generally split into N samples in order to be solved as an iterated map following Farmer's ideas.[13] Of course, Eq. (1) is not identical to the Ikeda DDE, but it is similar in having the same nonlinearity and bifurcation parameter b. Furthermore, the Ikeda DDE needs high values of b and τ (hence, high N) for high complexity, in contrast to Eq. (1), which needs only low b and high N values, as we will demonstrate next.

In Ref. 11, the CODEs of Eq. (1) were studied with respect to occasional paradigms and cases of selected values of N. It was shown that hyperchaos of order m (m positive Lyapunov exponents) can be generated by using $N=2m+1$ for the conservative case ($b=0$) in Eq. (1). Chaotic walks were also investigated for the conservative case for selected values of N. In this paper we expand this work by giving a detailed picture of Eq. (1) for the whole range: $3<N\leq 101$. The case $N=101$ is studied since it is a prime number and,

hence, prevents the system from breaking up into some number of smaller subsystems of lower dimension.

II. BIFURCATION SEQUENCE—ROUTE TO CHAOS

In this section we investigate the bifurcation sequence of Eq. (1). Analytic calculations (up to the fourth decimal digit) are carried out whenever possible as a check on the numerics that follow, especially since benchmarks for Lyapunov exponent calculations in high-dimensional chaotic systems are not widely available. This system has equilibria at

$$\sin x_{i+1}^* = b x_i^* \tag{2}$$

with eigenvalues λ that satisfy

$$(\lambda + b)^N = \prod_{i=1}^{N} \cos x_i^*. \tag{3}$$

For $b>1$, Eq. (2) has only a single solution, corresponding to an equilibrium at $x_i^*=0$ for all i, and thus the eigenvalues are given by the solutions of $(\lambda+b)^N=1$. The eigenvalues are real and are given by $\lambda=1-b$ for all N. The real parts of these eigenvalues are the Lyapunov exponents of the system.

As b decreases, the equilibrium at $x_i^*=0$ becomes unstable at $b=1$, and a pair of new stable symmetric equilibria are born in a pitchfork bifurcation with $bx^*=\sin x^* \cong x^* - x^{*3}/6$ or $x^* \cong \pm\sqrt{6(1-b)}$. From Eq. (3) with $\cos x^* = \sqrt{1-\sin^2 x^*} = \sqrt{1-b^2 x^{*2}}$, the eigenvalues of these new equilibria are given by

$$(\lambda + b)^N = [1 - b^2 x^{*2}]^{N/2} \tag{4}$$

with the real ones given simply by the $N/2$ root of Eq. (4):

$$\lambda^2 + 2b\lambda + b^2(1 + x^{*2}) - 1 = 0, \tag{5}$$

whose solutions are $\lambda=-b\pm\sqrt{1-b^2x^{*2}}$ for N even and $\lambda=-b+\sqrt{1-b^2x^{*2}}$ for N odd. For b only slightly less than 1.0, these eigenvalues are given approximately by $\lambda \cong -b \pm (3b-2)$ using the approximation for x^* above. The two real eigenvalues are equal when $1=\pm bx^*=\pm\sin x^*$ or $x^*=\pm\pi/2$ and $b=2/\pi$, and at that value of b, the largest Lyapunov exponent is $\lambda=-2/\pi$ and begins increasing as b decreases further.

What happens next as b decreases depends on whether N is odd or even. Consider first the case of N odd. In that case, the symmetric equilibria undergo a Hopf bifurcation when b reaches a value where $\lambda=\pm i\omega$ with a real part of zero, at which point a stable oscillation with frequency ω onsets. Substituting this value of λ into Eq. (3) and separately equating the real and imaginary parts on the two sides of the equation leads to

$$\sqrt{\omega^2 + b^2} = -\cos x^* \tag{6}$$

since N is odd and, hence, $\cos x^* < 0$, and

$$\omega = b \tan(\pi/N + 2n\pi/N) \tag{7}$$

with $n=0, \pm1, \pm2, \ldots$.

Equations (6) and (7) with $n=0$, when combined with Eq. (2), give a transcendental equation for x^*,

TABLE I. Hopf bifurcation for $N \geq 3$ and odd (selected values of N).

N	x^*	b	ω
3	2.288 930	0.328 990	0.569 828
5	2.102 313	0.410 043	0.297 914
7	2.064 155	0.426 687	0.205 481
9	2.049 680	0.432 999	0.157 599
11	2.042 602	0.436 085	0.128 046
21	2.032 493	0.440 492	0.066 394
31	2.030 466	0.441 376	0.044 884
41	2.029 733	0.441 695	0.033 911
51	2.029 388	0.441 846	0.027 252
61	2.029 198	0.441 929	0.022 780
71	2.029 083	0.441 979	0.019 569
81	2.029 007	0.442 012	0.017 152
91	2.028 956	0.442 034	0.015 266
101	2.028 918	0.442 051	0.013 754
Inf	2.028 758	0.442 121	$b\pi/N \to 0$

$$x^* \cos(\pi/N) + \tan x^* = 0 \tag{8}$$

with an approximate solution using a Taylor series of fourth order:

$$x^* = \pm 3\sqrt{1 + \cos(\pi/N)}.$$

Equation (8) can also be solved numerically using Newton's method to determine how x^* depends on N, from which b follows from

$$b = \sin x^*/x^* \tag{9}$$

and ω is given by Eq. (7). Results for some values of N are shown in Table I.

The case of $N=1$ is special because there is a single eigenvalue (and Lyapunov exponent), no Hopf bifurcation, and of course no chaos. For $b \geq 2/\pi$, the behavior is as described above. For $b<2/\pi$, the real eigenvalue is given by $\lambda=-b+\cos x^*$, which can be expanded about $b=0$, where $x^*=\pm\pi$. Taking the positive value as typical gives $\cos x^* \cong -1+(\pi-x^*)^2/2$. Furthermore, from Eq. (2), $bx^*=\sin x^* \cong \pi - x^*$, which gives $x^* \cong \pi/(1+b)$ and an eigenvalue

$$\lambda \cong -b - 1 + \frac{\pi^2 b^2}{2(1+b)^2}. \tag{10}$$

Note that $\lambda=-1$ for $b=0$ and that the equilibria become unstable ($\lambda=0$) when b reaches a negative value, given approximately by the root of the cubic equation

$$2b^3 + (6 - \pi^2)b^2 + 6b + 2 = 0, \tag{11}$$

for which the solution is $b \cong -0.2768$ and $x^* \cong \pm 4.3442$. The exact value of x^* is given by the solution of $\tan x^* = x^*$, which from Newton's method is $x^* \cong \pm 4.4934$ with $b=\sin x^*/x^* \cong -0.2172$, at which point a boundary crisis occurs[14,15] (the equilibrium points collide with their basins of attraction) and the trajectory becomes unbounded.

Now consider the case of N even. The behavior for $b \geq 2/\pi$ is the same as for N odd, with a pitchfork bifurcation at $b=1$ to a pair of symmetric equilibria. However, with decreasing b, rather than a Hopf bifurcation, there is a second pitchfork bifurcation when $\lambda=0$. This bifurcation occurs

TABLE II. Hopf bifurcation for $N \geq 6$ with $N/2$ odd (selected values of N).

N	x_a	x_b	b	ω
6	1.352 960	2.611 169	0.373 920	0.215 883
10	1.382 768	2.589 333	0.379 393	0.123 272
14	1.390 094	2.583 910	0.380 709	0.086 894
18	1.393 008	2.581 747	0.381 229	0.067 221
30	1.395 808	2.579 665	0.381 727	0.040 121
38	1.396 395	2.579 229	0.381 831	0.031 639
46	1.396 702	2.579 000	0.381 886	0.026 122
54	1.396 883	2.578 866	0.381 918	0.022 244
58	1.396 947	2.578 818	0.381 929	0.020 708
66	1.397 041	2.578 748	0.381 946	0.018 194
70	1.397 076	2.578 722	0.381 952	0.017 153
78	1.397 132	2.578 681	0.381 962	0.015 393
86	1.397 172	2.578 650	0.381 969	0.013 960
98	1.397 215	2.578 618	0.381 977	0.012 249
Inf	1.397 360	2.578 510	0.382 003	$b\pi/N \to 0$

when x^* satisfies Eq. (2) and (3) with $\lambda=0$, giving $\tan x^* = -x^*$ or $x^* \cong \pm 2.0287$ and $b = \sin x^*/x^* \cong 0.4421$ for all even N.

At this bifurcation point, a pair of asymmetric equilibria is born with $x_i^* = \pm x_a$ and $x_{i+1}^* = \pm x_b$ and a second pair with x_a and x_b interchanged. This is the first case with spatial structure (not all x_i are equal), and it corresponds to a spatial period doubling from period-1 to period-2 (adjacent spatial sites alternate in value). Because of the periodic boundary conditions, this behavior can occur only for even N. These new equilibria satisfy the conditions $\sin x_a = b x_b$ and $\sin x_b = b x_a$, and the eigenvalues are given by

$$(\lambda + b)^N = \cos^{N/2} x_a \cos^{N/2} x_b. \tag{12}$$

Just beyond the bifurcation point, the eigenvalue is real and is given by $\lambda = -b + \sqrt{\cos x_a \cos x_b}$. The largest two real eigenvalues exchange roles when $\cos x_a = 0$, which occurs when $x_a = \pm \pi/2$ and $x_b = \pm 1/b$. This condition is satisfied when $\sin x_b = \pi/2 x_b$, whose solution by Newton's method is $x_b \cong \pm 2.4433$ at $b \cong 0.4092$ with $\lambda = -b$.

What happens next depends on whether $N/2$ is even or odd (whether N is a multiple of 4). For $N/2$ odd, the next bifurcation is a Hopf and occurs for $\lambda = \pm i\omega$, where $\omega^2 + b^2 = -\cos x_a \cos x_b$ with ω given by Eq. (7). This system of transcendental equations in four variables (x_a, x_b, b, and ω) requires a numerical solution whose results (using a variant of simulated annealing) are shown in Table II. The case of $N=2$ is special because it does not undergo a Hopf bifurcation, but instead has a boundary crisis with $\lambda=0$ at $b=0$, where $x_a=0$ and $x_b = \pm\pi$.

Now consider the case of $N/2$ even. The behavior for $b \geq 0.4092$ is the same as for $N/2$ odd, but instead of undergoing a Hopf bifurcation as b decreases, it undergoes another pitchfork bifurcation with $\lambda=0$ when $b^2 = -\cos x_a \cos x_b$. Combined with $\sin x_a = b x_b$ and $\sin x_b = b x_a$ and solving numerically using a variant of simulated annealing, the result is $x_a \cong \pm 1.3973$, $x_b \cong \pm 2.5785$, and $b \cong 0.3820$.

At this bifurcation point, four asymmetric equilibria are born with $x_i^* = \pm x_a$, $x_{i+1}^* = \pm x_b$, $x_{i+2}^* = \pm x_c$, and $x_{i+3}^* = \pm x_d$, and three other cases with the values rotated. This case corresponds to a spatial period doubling from period-2 to period-4. Because of the periodic boundary conditions, this behavior can only occur for values of N that are multiples of 4 ($N/2$ must be even). These period doublings continue until a period-p is reached at which N/p is odd, and then a Hopf bifurcation occurs. The period doublings are analogous to the Feigenbaum sequence of period doublings in the logistic map and have the same scaling factor; i.e., $\delta = 4.6692\ldots$. However, these are pitchfork bifurcations rather than flips, since flips cannot occur in a continuous flow. In a pitchfork bifurcation, there are two stable branches, whereas in a flip, the two branches are individually unstable, but the orbit oscillates between the two in a stable period-2 cycle. The bifurcation sequence calculated for each of the cases above is summarized in Table III.

In calculating these attractors and their spectra of Lyapunov exponents, initial conditions are chosen throughout this paper to be uniform and random in the range of $-\pi$ to π range, and are not critical. However, as described in Ref. 9, if $x_1(0) = x_2(0) = \cdots = x_N(0)$, then the system behaves like a one-dimensional system with stable equilibria (point attractors) at $x_1^* = x_2^* = \cdots = x_N^*$.

Another way to view the expansion of the attractor with decreasing b is to plot the standard deviation of the trajectory from the origin

$$\sigma = \sqrt{\lim_{T\to\infty} \frac{1}{T} \int_0^T \sum_{i=1}^N x_i^2 dt} \tag{13}$$

along with the kurtosis[16]

$$k = \lim_{T\to\infty} \frac{1}{T\sigma^4} \int_0^T \sum_{i=1}^N x_i^4 dt - 3 \tag{14}$$

averaged along the trajectory, as shown in Fig. 1 for $N=101$. The kurtosis is defined such that a value of $k=0$ represents a normal (Gaussian) distribution, with a positive value indicating an enhanced tail and a negative value indicating a suppressed tail. The calculated negative value of $k \cong -2$ for all $b > 0$ indicates that the distribution is somewhat platykurtic (the tail of the distribution is truncated relative to a Gaussian). The standard deviation scales with b as $\sigma \approx 8/\sqrt{b}$. By the ergodic hypothesis,[17] these time averages are identical to the ensemble averages over many initial conditions and coarsely reflect the natural measure on the attractor apart from the fine-scale fractal structure.

III. DETERMINISTIC BROWNIAN MOTION

For the conservative case ($b=0$), the trajectory wanders ergodically and time-reversibly throughout the entire N-dimensional space (the "hyperlabyrinth"), except for the small quasiperiodic regions whose measure rapidly approaches zero with increasing N, where the trajectory drifts out parallel to one of the N axes. In Ref. 9, it was found that this percentage of the space for $N=3$ was $\Lambda(3) \cong 1.67\%$. After many calculations and verified for $N=4$, $\Lambda(4) \cong 0.028\%$ according to Eq. (15), and it is conjectured herein that this fraction follows the relation for $N > 1$:

TABLE III. Summary of bifurcation sequence

Dynamic	b	x^*	λ
	$N=1$		
Stable equilibrium	>1	0	$1-b$
Pitchfork bifurcation	1	0	0
Bistable equilibria	<1	$\sin x^*=bx^*$	$-b-1+\cos x^*$
Boundary crisis	−0.2172…	±4.4934…	0
	$N=2$		
Dynamic	b	x^*	λ
Stable equilibrium	>1	0	$1-b$
Pitchfork bifurcation	1	0	0
$\lambda_1=\lambda_2$	$2/\pi$	$\pm\pi/2$	$-2/\pi$
Pitchfork bifurcation	0.4421…	±2.0287…	0
$\lambda_1=\lambda_2$	0.4092…	$\pm\pi/2,\pm1/b$	$-b$
Boundary crisis	0	$\pm\pi$, 0	0
	$N\geq3$ and odd		
Dynamic	b	x^*	λ
Stable equilibrium	>1	0	$1-b$
Pitchfork bifurcation	1	0	0
$\lambda_1=\lambda_2$	$2/\pi$	$\pm\pi/2$	$-2/\pi$
Hopf bifurcation	See Table I	See Table I	See Table I
	$N\geq6$ with $N/2$ odd		
Dynamic	b	x^*	λ
Stable equilibrium	>1	0	$1-b$
Pitchfork bifurcation	1	0	0
$\lambda_1=\lambda_2$	$2/\pi$	$\pm\pi/2$	$-2/\pi$
Pitchfork bifurcation	0.4421…	±2.0287…	0
$\lambda_1=\lambda_2$	0.4092…	$\pm\pi/2,\pm1/b$	$-b$
Hopf bifurcation	See Table II	See Table II	See Table II
	$N\geq4$ with $N/2$ even		
Dynamic	b	x^*	λ
Stable equilibrium	>1	0	$1-b$
Pitchfork bifurcation	1	0	0
$\lambda_1=\lambda_2$	$2/\pi$	$\pm\pi/2$	$-2/\pi$
Pitchfork bifurcation	0.4421…	±2.0287…	0
$\lambda_1=\lambda_2$	0.4092…	$\pm\pi/2,\pm1/b$	$-b$
Pitchfork bifurcation	0.3820…	±1.3973…	0
		±2.5785…	
$\lambda_1=\lambda_2$	0.3760…	$\pm\pi/2,\pm1/b$	$-b$
		±1.2340…	
		±2.5096…	
	Feigenbaum	until N/p	
Pitchforks or Hopf	cascade	becomes odd	

$$\Lambda(N)\cong 0.0167^{N-2}. \tag{15}$$

Note that $\Lambda(2)=1$, and all initial conditions give periodic orbits as expected. As N increases, then $\Lambda(N\to\infty)$ tends to zero, meaning that all initial conditions lead to chaotic solutions.

Note that the divergence of the flow given as

$$\nabla\cdot\mathbf{v}=\sum_{i=1}^{N}\frac{\partial}{\partial x_i}\sin x_{i+1}\equiv 0 \tag{16}$$

is identically zero, which means that the flow is incompressible and, hence, of constant density throughout the ergodic region. Given the uniform measure, it is simple to calculate the root-mean-square speed

$$v_{\rm rms}=\sqrt{\sum_{i=1}^{N}\overline{\sin^2 x_i}}=\sqrt{N/2}, \tag{17}$$

each component of which is $1/\sqrt{2}$.

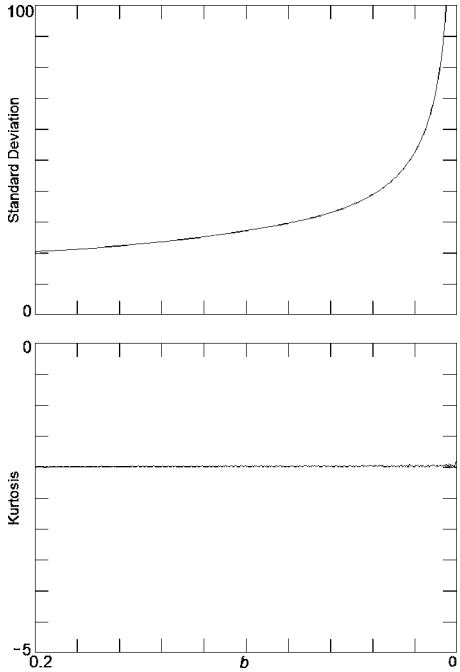

FIG. 1. Standard deviation and kurtosis for the excursion of the trajectory from the origin for the attractors as a function of b with $N=101$.

However, the approach to this equilibrium is by way of a diffusion, reminiscent of Brownian motion, but in a purely deterministic system. The trajectory for one such typical case with $N=101$ is shown in Fig. 2 projected onto the x_1-x_2 plane. For a collection of 1.6×10^6 initial conditions that start at random positions near the origin, the probability distribution function along each of the 101 axes after a time lapse of 4×10^3 is shown in Fig. 3. Also shown in the figure in red is a Gaussian distribution with the same standard deviation ($\sigma\cong63.4$) and area. The observed distribution is closely Gaussian with a negligible kurtosis of $k\cong-0.003$, in contrast to the strongly leptokurtic (fat-tailed) distribution ($k\cong9.8$) found for $N=3$ and $b=0$[9] and the slightly platykurtic (thin-tailed) distribution ($k\cong-2$) for $N=101$ and $b>0$. Thus, the behavior is identical to a random walk produced by steps that are independent and identically distributed.

Figure 4 shows the standard deviation versus time for 1.6×10^4 initial conditions uniform over a 101-dimensional hypercube centered on the origin and extending from −0.1 to 0.1 along each axis. The slope of the least-squares fitted curve (0.508) over the range $8\leq t\leq8192$ indicates that the motion is closely Brownian (for which the slope would be 0.5).[18] These results contrast with the simplest labyrinth-chaos case of $N=3$, where fractional Brownian motion with a slope of 0.61 was observed. The latter shows that with increasing N, the slope, which coincides with the Hurst expo-

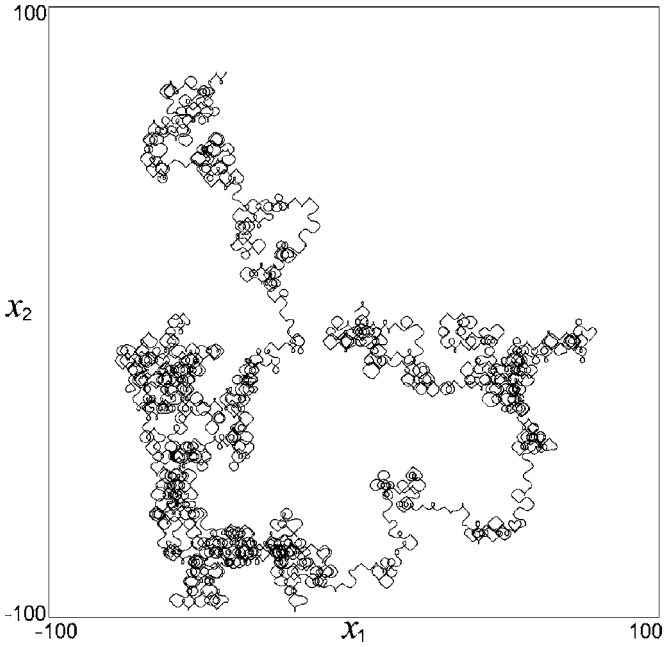

FIG. 2. Brownian motion (chaotic "walk") of a trajectory in the chaotic sea for $b=0$ and $N=101$ projected onto the x_1-x_2 plane.

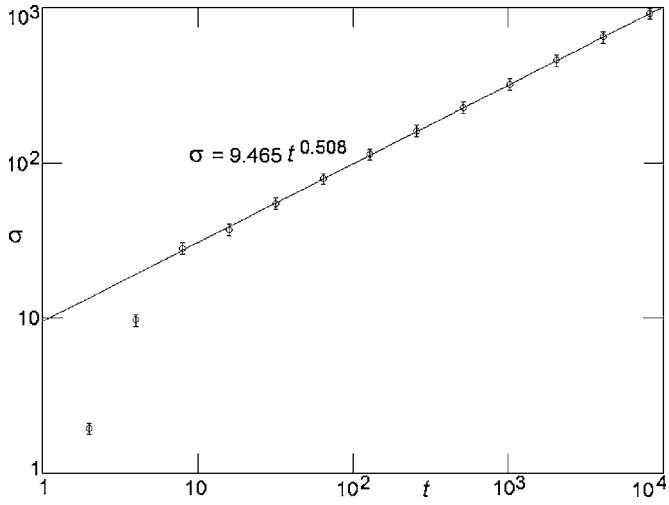

FIG. 4. Standard deviation of 1.6×10^4 trajectories starting near the origin versus time for $b=0$ and $N=101$.

nent as defined below, decreases, resulting in a higher fractal dimension and less long-term memory (see Ref. 19 and references therein).

From the best fit linear regression of $\log_{10}\sigma$ versus $\log_{10} t$ given by $\sigma=9.465t^{0.508}$ and assuming $\sigma=(t/\tau)^H d$, where τ is an effective collision time and d is an effective mean free path with $d/\tau=v$ given by Eq. (18), one obtains $\tau=(9.465/7.106)^{1.969}\cong 1.758$ and $d=7.106\times 1.758\cong 12.5$, which is about twice the lattice size of 2π, whereas one might have expected the mean free path to be approximately equal to the lattice size. The quantity H (=0.508 in this case) is called the Hurst exponent.[20] The corresponding values for $N=3$ are $\tau\cong 0.68$ and $d\cong 0.83$.

An alternate calculation of the Hurst exponent follows a single trajectory for a very long time with the rescaled range R/S plotted versus time on a log-log plot, the slope of which is H.[17,21] The range R is the maximum excursion from the starting point, and S is the average step size (approximately the mean free path d), which does not depend on time. Hence, it suffices just to plot $\log_{10} R$ versus $\log_{10} t$, as shown in Fig. 5, where the slope of the best fit straight line over for $t>10$ is $H=0.527$ for $N=101$, in good agreement with the value of 0.508 obtained from Fig. 4 and in contrast to the value of $H=0.62$ found by this same method with $N=3$. In Fig. 5 the initial conditions were taken as $x_1(0)=0.2$ and $x_i(0)=0$ for $i>1$, and the trajectory was followed for a time of 10^8 with a fourth-order Runge–Kutta step size of 0.05.

Figure 6 shows the autocorrelation function

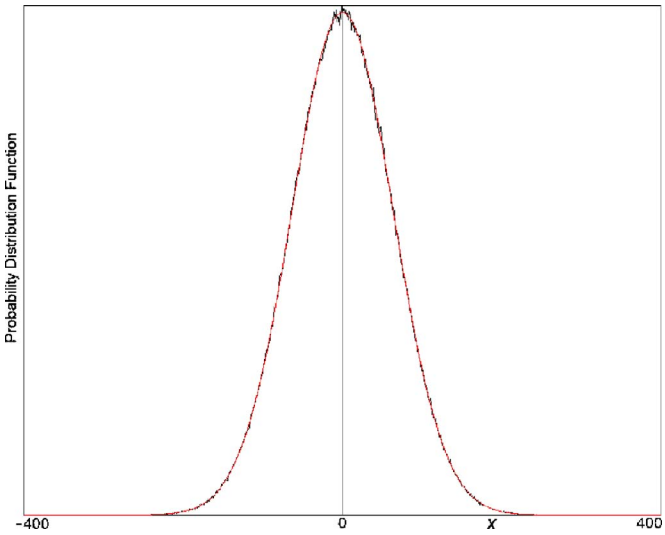

FIG. 3. Probability distribution function for each component of x for 1.6×10^6 initial conditions near the origin after a time of 4×10^3 with $b=0$ and $N=101$. The red curve is a Gaussian distribution with the same standard deviation and area.

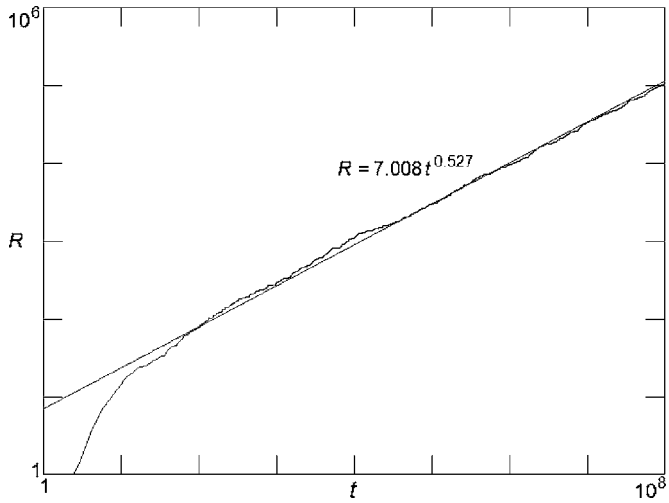

FIG. 5. Range vs time for $b=0$ and $N=101$ showing a Hurst exponent of $H=0.527$.

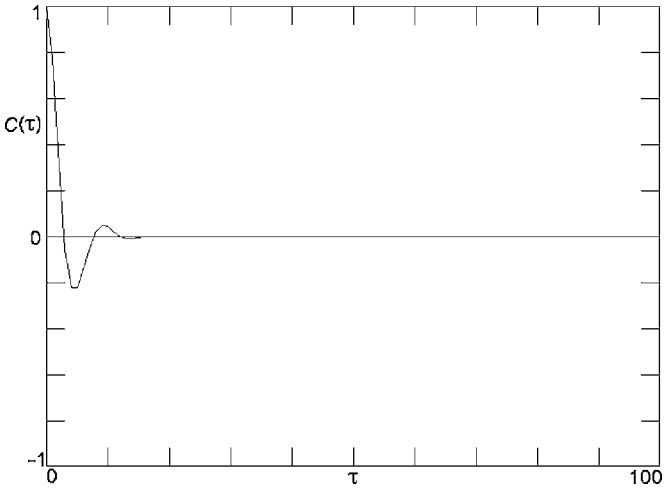

FIG. 6. Autocorrelation function of $\dot{x}$ vs delay for $b=0$ and $N=101$.

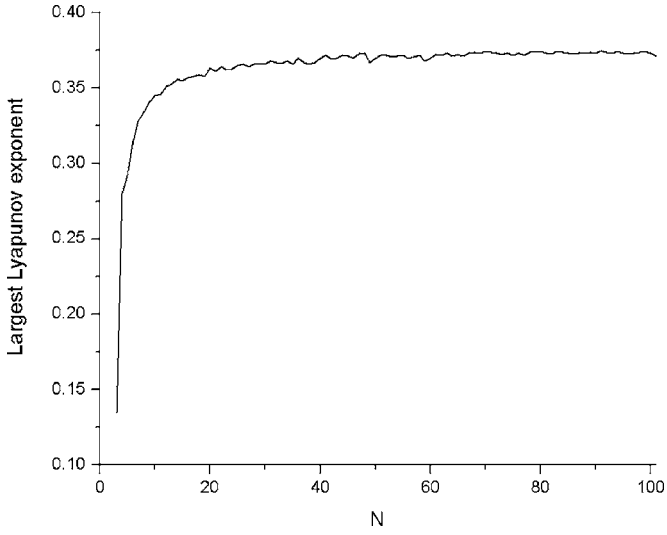

FIG. 7. Largest Lyapunov exponent versus N for $b=0.05$.

$$C(\tau)=\frac{\int_{\tau}^{\infty}\dot{x}(t)\dot{x}(t-\tau)dt}{\int_{\tau}^{\infty}\dot{x}(t)^2dt} \tag{18}$$

for the same trajectory as in Fig. 5, showing the short-term correlation that falls rapidly to zero, as expected for a truly random process. The function appears to be an exponentially decaying oscillation. The autocorrelation function is the Fourier transform of the power spectral density[22] and was performed on the time derivative of x rather than x itself because the time derivative of a random walk is expected to be uncorrelated (white) noise, as appears to be the case.

IV. SCALING LAWS

The system of Eq. (1) can be considered as a coupled system of flows. In Ref. 9, it was shown for what values of b chaos occurs with $N=3$. In this section we will examine—as an obvious extension—the scaling laws for the largest Lyapunov exponent (LLE), the Kaplan–Yorke dimension D_{KY},[23] and the metric (Kolmogorov–Sinai) entropy h_{KS} in the high-dimensional limit $3<N\leq 101$. Only the bifurcation parameter b is kept constant at $b=0.05$ as N varies. This value of b was chosen since it is close to the conservative ($b=0$) case.

In Fig. 7, the LLE is plotted as a function of N. The value of the LLE is approximately constant for high values of N, despite the fact that the dimension and the metric entropy are increasing, as will be shown next. After approximately $N>40$, the LLE approaches asymptotically its upper limit value of about 0.374. The Kaplan–Yorke dimension D_{KY} and the metric entropy h_{KS} increase linearly as N increases, following the relations (by calculating D_{KY} and h_{KS} with a step of $\delta N=5$ for $3<N\leq 101$ and applying a least-squares fit)

$$D_{\mathrm{KY}}\cong 0.892N-0.022, \tag{19}$$

$$h_{\mathrm{KS}}\cong 0.09N-0.038 \tag{20}$$

with an R^2 value equal to 0.99, meaning that the dependence of these quantities on N is linear. (The R^2 value, where $0\leq R^2\leq 1$, is defined as the measure of a least-squares fit with $R^2=1$ signifying a perfect linear correlation.) Furthermore, for $b=0$ (the conservative case) the dimension is equal to N, and the metric entropy follows the relation

$$h_{\mathrm{KS}}\cong 0.11N-0.08 \tag{21}$$

From Eqs. (19)–(21), it is shown that the system for decreasing b becomes more complex (higher dimension for higher a_1 from the slope of $D_{KY}=a_1N+a_2$) and more chaotic (higher metric entropy for higher c_1 from the slope of $h_{\mathrm{KS}}=c_1N+c_2$). In order to verify that result, for $b=0.18$, we calculate $a_1=0.678$ and $c_1=0.052$, values lower than the case of $b=0.05$ and $b=0$.

Another interesting result is that for any chaotic case for a set of values (b,N), the slopes discussed above follow the equations

$$dD_{\mathrm{KY}}/dN\cong -1.758b+0.992, \tag{22}$$

$$dh_{\mathrm{KS}}/dN\cong -0.316b+0.108, \tag{23}$$

since the values of the intercepts were not fitted. By setting the two equations above equal to zero, we find that in order to have positive slopes for a chaotic case, we require $b<0.34$. Hence, independent of N, b should always be less than 0.34. From Eqs. (22) and (23), we can extract general equations for the scaling laws given by

$$D_{\mathrm{KY}}\cong(-1.758b+0.992)N+\varepsilon, \tag{24}$$

$$h_{\mathrm{KS}}\cong(-0.316b+0.108)N+\xi, \tag{25}$$

where $|\varepsilon|$ and $|\xi|$ are small constants less than 0.1 in all tested cases. Note, though, that since D_{KY} is two orders of magnitude larger than ε and h_{KS} is only one order of magnitude larger, then Eq. (24) results in a more accurate general scaling law than does Eq. (25), especially for small N.

For $N=4$, no hyperchaos (two or more positive Lyapunov exponents) was found for the whole range of b, as one might have expected. The latter might have to do with the limited number of variables of this four-dimensional system of ODEs, but generally there are no criteria for having

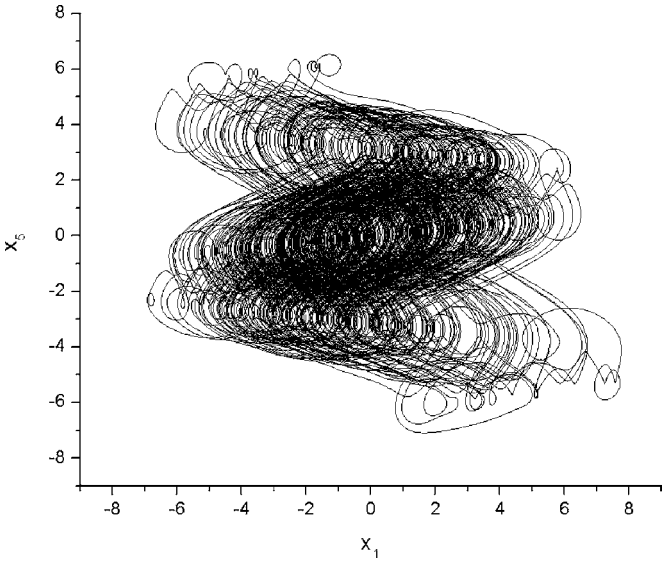

FIG. 8. Phase portrait of x_1 vs x_5 showing the first hyperchaotic case for $b=0.108$ with $N=5$.

hyperchaos in chaotic flows except for the minimum number of equations ($N=4$). The first hyperchaotic case was found for $(b,N)=(0.108,5)$ with an LE spectrum of (0.252, 0.009, 0, −0.308, −0.5) and $D_{KY}=3.857$ and shown with a filled circle in Fig. 9. Figure 8 shows the phase portrait of x_1 versus x_5 (and is very similar to the Ikeda DDE attractor), and Fig. 9 shows the first four Lyapunov exponents versus b for $N=5$. Note that for low values of b, the system becomes more chaotic and more complex, and this holds for the whole range of (b,N) values.

As was shown in Eqs. (24) and (25), the metric entropy and dimension increase linearly with N for any b. In both the Ikeda DDE[5] and the Mackey–Glass DDE,[13] the dimension increases linearly with the delay time τ, but the entropy approaches a constant value. Hence, Eq. (1) in its high-dimensional limit could serve as a more complex prototypical minimal system in contrast to simple DDEs since its chaoticity (entropy) increases simultaneously with its complexity (dimension).

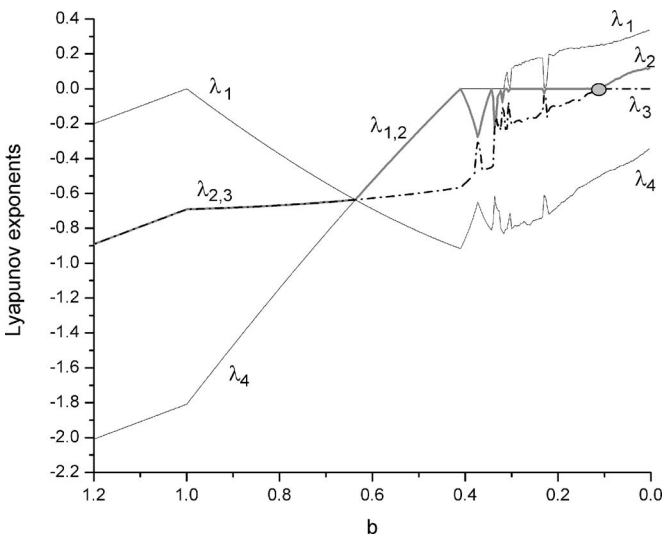

FIG. 9. Lyapunov exponents λ_1, λ_2, λ_3, and λ_4 vs b for $N=5$. The filled circle denotes the point for $b=0.108$, where the second Lyapunov exponent becomes positive (hyperchaos). Notation $\lambda_{\alpha,\beta}$ means that Lyapunov exponents λ_α and λ_β coincide up to the second decimal digit with $\lambda_\alpha > \lambda_b$. λ_5 was not plotted since it is very negative.

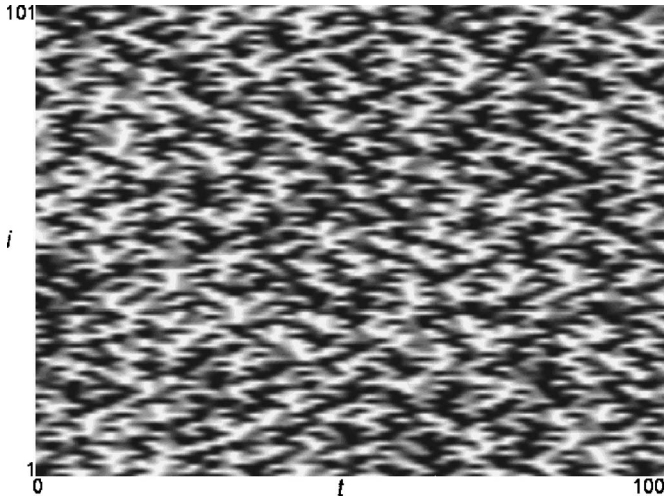

FIG. 10. Spatiotemporal plot of $\sin x_i(t)$ for $b=0$ and $N=101$, showing the broken symmetry and propagating chaotic structures.

V. DISCUSSION AND CONCLUSIONS

The system in Eq. (1) provides an interesting and simple example of a high-dimensional chaotic system. It can be viewed as a ring of interacting agents, with each agent driven nonlinearly by only the one on its right, or as a single chaotic trajectory on an N-torus or in a spatially infinite N-dimensional hyperlabyrinth. The first description provides a model of one-dimensional spatiotemporal chaos in which there is spontaneous symmetry breaking. Whereas the governing equations are symmetric with respect to a rotation of the ring, the solution is not, as indicated by the spatiotemporal plot in Fig. 10. In this figure with $N=101$ and $b=0$, a gray scale is used to indicate the value of $\sin x_i$ at each of the 101 values of i as time advances, with white corresponding to −1 and black to +1. The plot shows coherent structures that grow, propagate, and then dissipate in an apparently chaotic manner. The plot actually starts at a time of $t=400$ to eliminate an initial transient during which the structures self-organize despite the absence of an attractor for this Hamiltonian system. By "Hamiltonian" we mean that the trace of the Jacobian matrix, and thus the sum of all N Lyapunov exponents, is zero and, hence, there is no dissipation.

In conclusion, the hyperlabyrinth system of Eq. (1), despite its simplicity and elegance, shows rich dynamical behavior. From Ref. 11, it is known, and verified herein, that m positive Lyapunov exponents appear by using $N=2m+1$ for $b=0$. We extended this result further by calculating the scaling laws of D_{KY} and h_{KS} as a function of N and also b, since the number of positive Lyapunov exponents m does not by itself give any information about the complexity and chaoticity of the system, especially at large N. This system could serve as a prototypical example of a high-dimensional chaotic system in contrast, for example, to chaotic delay differ-

ential equations or diffusively coupled systems[24] when the Lyapunov dimension and the Kolmogorov–Sinai entropy are considered. With the reported numerical results in this paper and the stability analysis, one can easily produce a wide variety of chaotic states. Finally, it was shown that this system in its high-dimensional limit produces chaotic walks with behavior identical to a random walk produced by steps that are independent and identically distributed. The latter was found by calculating the Hurst exponent H, revealing that as N increases the system has less long-term memory, with each data point less correlated with preceding values (H is very close to 0.5). Hence, Eq. (1) is a very simple, elegant, and prototypical high-dimensional system with likely relevance to some natural systems.

ACKNOWLEDGMENT

One of us (K.E.C.) is supported by the EU project PIC-ASSO IST-2005-34551.

[1]D. Mackey and L. Glass, Science **197**, 28 (1977).
[2]D. Michelson, Physica D **19**, 89 (1986).
[3]J. C. Sprott, Phys. Lett. A **228**, 271 (1997).
[4]K. E. Chlouverakis and J. C. Sprott, Chaos, Solitons Fractals **28**, 739 (2005).
[5]K. Ikeda and K. Matsumoto, Physica D **29**, 223 (1987).
[6]J. C. Sprott, Electronic Journal of Theoretical Physics **3**, 19 (2006).
[7]E. A. Jackson and A. Kodogeorgiou, Phys. Lett. A **168**, 270 (1992).
[8]R. Thomas, Int. J. Bifurcation Chaos Appl. Sci. Eng. **9**, 1889 (1999).
[9]J. C. Sprott and K. E. Chlouverakis, Int. J. Bifurcation Chaos Appl. Sci. Eng.(to be published).
[10]M. W. Hirsch and S. Smale, *Differential Equations, Dynamical Systems and Linear Algebra* (Academic, New York, 1974).
[11]R. Thomas, V. Basios, M. Eiswirth, T. Kruel, and O. E. Rossler, Chaos **14**, 669 (2004).
[12]V. S. Udaltsov, J.-P. Goedgbuer, L. Larger, and W. T. Rhodes, Phys. Rev. Lett. **86**, 1892 (2001).
[13]J. D. Farmer, Physica D **4**, 366 (1982).
[14]C. Grebogi, E. Ott, and J. A. Yorke, Phys. Rev. Lett. **48**, 1507 (1982).
[15]C. Grebogi, E. Ott, and J. A. Yorke, Physica D **7**, 181 (1983).
[16]W. H. Press, B. P. Flannery, S. A. Teukolsky, and W. T. Vetterling, *Numerical Recipes: The Art of Scientific Computing*, 2nd ed. (Cambridge University Press, Cambridge, 1992).
[17]D. Ruelle, Am. J. Math. **98**, 619 (1976).
[18]R. A. Feagin, Physica A **328**, 315 (2003).
[19]C. Yanqing, D. Mingzhou, and J. A. Scott Kelso, Phys. Rev. Lett. **79**, 4501 (1997).
[20]H. E. Hurst, R. P. Black, and Y. M. Simaika, *Long-Term Storage: An Experimental Study* (Constable, London, 1965).
[21]J. Feder, *Fractals* (Plenum, New York, 1988).
[22]L. W. Couch, *Digital and Analog Communications Systems*, 6th ed. (Prentice Hall, Englewood Cliffs, NJ, 2001), pp. 406–409.
[23]J. Kaplan and J. Yorke, Lect. Notes Math. **730**, 228 (1979).
[24]L. Kocarev and U. Parlitz, Phys. Rev. Lett. **77**, 2206 (1996).